Inflammatory Mediators Increase Nav1.9 Current and Excitability in Nociceptors through a Coincident Detection Mechanism

François Maingret,[1] Bertrand Coste,[1] Françoise Padilla,[1] Nadine Clerc,[1] Marcel Crest,[1] Sergiy M. Korogod,[2] and Patrick Delmas[1]

[1]CRN2M, CNRS, Université de la Méditerranée, 13916 Marseille Cedex 20, France
[2]Laboratory of Biophysics and Bioelectronics, Dniepropetrovsk National University, 49050 Dniepropetrovsk, Ukraine

Altered function of Na^+ channels is responsible for increased hyperexcitability of primary afferent neurons that may underlie pathological pain states. Recent evidence suggests that the Nav1.9 subunit is implicated in inflammatory but not acute pain. However, the contribution of Nav1.9 channels to the cellular events underlying nociceptor hyperexcitability is still unknown, and there remains much uncertainty as to the biophysical properties of Nav1.9 current and its modulation by inflammatory mediators. Here, we use gene targeting strategy and computer modeling to identify Nav1.9 channel current signature and its impact on nociceptors' firing patterns. Recordings using internal fluoride in small DRG neurons from wild-type and Nav1.9-null mutant mice demonstrated that Nav1.9 subunits carry the TTX-resistant "persistent" Na^+ current called NaN. Nav1.9$^{-/-}$ nociceptors showed no significant change in the properties of the slowly inactivating TTX-resistant SNS/Nav1.8 current. The loss in Nav1.9-mediated Na^+ currents was associated with the inability of small DRG neurons to generate a large variety of electrophysiological behaviors, including subthreshold regenerative depolarizations, plateau potentials, active hyperpolarizing responses, oscillatory bursting discharges, and bistable membrane behaviors. We further investigated, using CsCl- and KCl-based pipette solutions, whether G-protein signaling pathways and inflammatory mediators upregulate the NaN/Nav1.9 current. Bradykinin, ATP, histamine, prostaglandin-E2, and norepinephrine, applied separately at maximal concentrations, all failed to modulate the Nav1.9 current. However, when applied conjointly as a soup of inflammatory mediators they rapidly potentiated Nav1.9 channel activity, generating subthreshold amplification and increased excitability. We conclude that Nav1.9 channel, the molecular correlate of the NaN current, is potentiated by the concerted action of inflammatory mediators that may contribute to nociceptors' hyperexcitability during peripheral inflammation.

INTRODUCTION

A variety of different Na^+ channel subunits (Nav) are expressed in the subset of primary afferent neurons involved in the generation of pain sensation. Adult dorsal root ganglion (DRG) neurons express at least five Nav subtypes (Nav1.1 and Nav1.6–Nav1.9). Among them, Nav1.8 and Nav1.9 contain a structural motif common to tetrodotoxin-resistant (TTX-R) Nav channels and are thought to play specialized roles in pain pathways since they are preferentially expressed in nociceptive DRG neurons giving rise to C and Aδ fibers (Dib-Hajj et al., 1998; Amaya et al., 2000; Benn et al., 2001; Fang et al., 2002; Fang et al., 2006; Coste et al., 2007). Gene targeting and heterologous expression studies have shown that Nav1.8 encodes a slowly inactivating TTX-R Na^+ current known as SNS (sensory neuron specific) current (Akopian et al., 1996). This current has a relatively depolarized activation threshold and may support action potential electrogenesis in nociceptors (Renganathan et al., 2001; Blair and Bean, 2002). On the other hand, the Na^+ current mediated by Nav1.9 has not been definitely identified, since its expression in exogenous systems has not been conclusive. Human Nav1.9 expressed in HEK-293 cells did not open in response to depolarization (Blum et al., 2002). Indeed, opening was only achieved through BDNF or neurotrophin-4/5 receptor activation, suggesting that Nav1.9 may be gated by extracellular ligands rather than by voltage. In nociceptors, however, the body of evidence suggests that Nav1.9 carries the NaN (novel and nociceptive) current (Dib-Hajj et al., 1998; Cummins et al., 1999; Fjell et al., 1999; Delmas and Coste, 2003; Priest et al., 2005). NaN channels have a more hyperpolarized activation threshold than SNS/Nav1.8 channels and give rise to a prominent persistent Na^+ current at subthreshold voltages, which may regulate subthreshold excitability in small DRG neurons (Cummins et al., 1999; Coste et al., 2004; Maruyama et al., 2004; Coste et al., 2007). In addition, the NaN current displays slow activation kinetics, which makes

F. Maingret and B. Coste contributed equally to this work.
Correspondence to Patrick Delmas: patrick.delmas@univmed.fr
The online version of this article contains supplemental material.

Abbreviations used in this paper: BK, bradykinin; DRG, dorsal root ganglion; NaN, novel and nociceptive; Nav, Na^+ channel subunits; SNS, sensory neuron specific; TTX, tetrodotoxin.

J. Gen. Physiol. © The Rockefeller University Press $30.00
Volume 131 Number 3 March 2008 211–225
http://www.jgp.org/cgi/doi/10.1085/jgp.200709935

unlikely its contribution to action potential upswing (Herzog et al., 2001; Blair and Bean, 2002).

Previous studies using Nav1.9-null mutant mice provided evidence to suggest that Nav1.9 subunits contribute to thermal as well as mechanical hypersensitivities after inflammation (Priest et al., 2005; Amaya et al., 2006). These findings are consistent with our recent observation that the NaN current is expressed in nociceptors functionally classified as thermo- and mechanonociceptors (Coste et al., 2007). In support to a role in nociceptor sensitization, the Nav1.9 subunit has been localized in unmyelinated nerve endings innervating sensory territories susceptible to undergo inflammatory hyperalgesia such as the cornea (Black and Waxman, 2002), the lips skin, and the dental pulp (Padilla et al., 2007). However, little information is available regarding the action of inflammatory mediators on NaN channel activity. There is some evidence to suggest that inflammatory mediators, including prostaglandin-E2 (PGE2) and serotonin, modulate TTX-R Na^+ currents in DRG neurons, but the specific role of the different Na^+ channel subtypes has not been established (England et al., 1996; Gold et al., 1996; Gold et al., 1998; Khasar et al., 1998; Kwong and Lee, 2005). With regard to NaN current, PGE2 has been shown to have no detectable effect when applied acutely (Zheng et al., 2007) contrary to report that showed upregulation after 1 h preincubation (Rush and Waxman, 2004).

Accordingly, in the present study we used a combination of electrophysiological characterization of TTX-R Na^+ currents in wild-type and Nav1.9 knock-out mouse DRG neurons and computer modeling methods to determine the contribution of Nav1.9 dependent Na^+ currents to the electrical activity of DRG neurons and to enhanced excitability produced by inflammatory agents. We demonstrate that Nav1.9 channels carry the NaN current and contribute to a variety of electrophysiological behaviors including plateau potentials, oscillatory bursting activities and conditional bistable behaviors. Moreover, we show that concurrent activation of inflammatory mediator receptors enhances NaN/Nav1.9 current, lowering threshold for excitability. Collectively, our data indicate that Nav1.9 is upregulated by the concerted action of inflammatory mediators, which may contribute to nociceptor hyperexcitability during peripheral inflammation.

MATERIALS AND METHODS

All procedures were in accordance with the directives of the French Ministry of Agriculture and Fisheries and the European Communities Council (86/609/EEC).

Generation of Nav1.9$^{-/-}$ Mice and Genotyping

Heterozygous mice were generated by Glaxo Smith Kline. In brief, a 129/Ola mouse genomic library was screened to isolate genomic sequence of Nav1.9 (*Scn11a*, NM_011887). A 10.8-kb fragment encoding exons 5–10 was used to generate the targeting vector. An IRES/LacZpA cassette followed by a loxP/neo/loxP cassette was inserted into the end of exon 5, resulting in the deletion of exons 6 and 7 of the *Scn11a* gene. A double MC1-tk-pA herpes simplex virus thymidine kinase expression cassette was added to enrich for homologous recombinants by negative selection with 1-(2-desoxy-2-fluoro-β-D-arabinofuranosyl)-S-iodouracil. Targeting construct was electroporated into E14-Tg2a-IV embryonic stem (ES) cell line. G418-5 fialuridine–resistant ES cell clones were selected and verified for homologous recombination at the *Scn11a* locus by Southern blot analysis. These clones were injected into C57BL/6 blastocysts, and the resulting chimeras were mated with C57BL/6 females to generate heterozygous animals harboring one knockout allele of Nav1.9. Heterozygous mice were subsequently crossed with wild-type C57BL/6 mice (Nav1.9$^{+/+}$) to generate the homozygous Nav1.9-null mice (Nav1.9$^{-/-}$) employed in the present study.

Mice colonies were genotyped by PCR from tail biopsy samples. PCR amplification of the wild-type *Scn11a* allele used the FW (5′-tgctttgtagatacgtcttcattgg-3′) and RW (5′-accatactgtgactagcattaatcctc-3′) primer pairs and resulted in a 490-bp amplicon. PCR amplification of the disrupted *Scn11a* allele used the FM (5′-aatgggctgaccgcttcctcgtg-3′) and RM (5′-caaagctggacaagactcagctatg-3′) primer pairs and gave a 380-bp fragment product.

Acutely Dissociated DRG Neurons

Dissociation of DRG neurons has been previously described (Coste et al., 2004; Coste et al., 2007). In brief, cultures of thoraco-lumbar DRG neurons were established from young male mice (C57BL/6 and Nav1.9$^{-/-}$). Excised DRG ganglia were incubated in enzyme solution containing 2 mg/ml of collagenase IA (Invitrogen) for 45 min at 37°C and triturated in Hanks' medium (Invitrogen). Culture medium was Dulbecco's modified Eagle's medium (DMEM) supplemented with 10% heat-inactivated fetal calf serum, 100 U/ml penicillin-streptomycin, 2 mM L-glutamine, 25 ng/ml nerve growth factor (NGF), and 2 ng/ml glial-derived neurotrophic factor (GDNF) (all from Invitrogen). Cells were maintained in a humidified atmosphere (5% CO_2, 37°C) for 4–12 h before recording.

Electrophysiology

Patch pipettes had resistances of 1.9–2.5 and 2.5–3.2 MΩ for whole-cell voltage clamp and current clamp recordings, respectively. Intracellular solutions used in this study are listed in Table I. For voltage clamp recording of Na^+ currents, extracellular solution had a reduced driving force for Na^+ (in mM): 60 NaCl, 110 sucrose, 3 KCl, 1 $MgCl_2$, 10 HEPES, 2.5 $CaCl_2$, 10 glucose, 10 TEA-Cl, 0.0005 TTX (pH 7.4, 305 mOsm/l). For dual (voltage and current clamp) recordings, the extracellular solution had a standard driving force for Na^+ and consisted of (in mM) NaCl 120, 3 KCl, 1 $MgCl_2$, 10 HEPES, 2.5 $CaCl_2$, 10 glucose (pH 7.4, 305 mOsm/liter). Except in Fig. 8, all extracellular solutions contained 500 nM tetrodotoxin (TTX) as well as 1 mM amiloride and 5 μM La^{3+} in order to block Ca^{2+} currents without altering NaN/Nav1.9 properties (Coste et al., 2007). The resting membrane potential (wild type, −63.4 ± 1.5 mV, n = 12; Nav1.9$^{-/-}$, −63.2 ± 1.4 mV, n = 10) and the input resistance (wild type, 670 ± 48 MΩ, n = 12; Nav1.9$^{-/-}$, 789 ± 80 MΩ, n = 10) were measured with KCl-based patch pipette solution (solution 5, Table I) and were not significantly different between small Nav1.9$^{+/+}$ and Nav1.9$^{-/-}$ DRG neurons.

Data Acquisition and Analysis

Data were acquired with an Axopatch 200B amplifier (Axon Instruments), filtered at 2 kHz, and digitally sampled at 20–50 kHz using PCLAMP 8.02 software. Except for voltage-ramp protocols, currents were leak subtracted using a P/6 protocol. Voltage errors

TABLE I

Composition of Intracellular solutions

	CsCl	CsF	KCl	EGTA	$CaCl_2$	NaCl	$MgCl_2$	Na_2GTP	MgATP	HEPES	Figs.
Solution 1	100	30	0	10	1	8	1	0.4	4	10	2 (A and B) and 3
Solution 2	0	30	100	10	1	8	1	0.4	4	10	1 and 4
Solution 3	130	0	0	10	1	8	1	0.4	4	10	5 and 6
Solution 4	30	0	100	10	1	8	1	0.4	4	10	7
Solution 5	0	0	130	10	1	8	1	0.4	4	10	8

Concentrations are expressed in mM. pH adjusted to 7.3 with NaOH, 300 mOsm/liter.

were minimized using 70–85% series resistance compensation. Whole-cell recording were begun 5 min after achieving the whole-cell configuration, to allow Cs^+ to equilibrate and to allow NaN channels to recover from slow inactivation. NaN/Nav1.9 current was typically measured between −50 and −60 mV where SNS/Nav1.8 current was absent. Conductance–voltage curves were calculated from the peak current according to the equation $G = I/(V - E_{rev})$, where V is the test pulse potential and E_{rev} the reversal potential calculated according to the Nernst equation. The activation curve (G–V) was fitted using the Boltzmann function: $G/G_{max} = 1/(1 + \exp[(V_{1/2} - V)/k])$, where G/G_{max} is the normalized conductance, $V_{1/2}$ is the potential of half-maximum channel activation, and k is the steepness factor.

PRISM 4.0 (GraphPad) software was used to perform linear and nonlinear fitting of data. Results are presented as mean ± SEM and *n* represents the number of cells examined. Statistical analysis used Student's *t* test and $P < 0.05$ was considered statistically significant.

Drug Application

All experiments were performed at room temperature and chemicals were obtained from Sigma-Aldrich (except TTX, Alomone Laboratories). Extracellular media were exchanged using a gravity-fed bath perfusion system at a flow rate of 2–5 ml/min, while bath solution was removed by continuous suction. Recycling was used to reduce the amount of TTX used. Stock solutions of TTX (0.1 mM) and La^{3+} (100 mM) were prepared in water. Stock solution of amiloride hydrochloride (1 M) was made in dimethylsulphoxide (final concentration, 0.1%). A stock solution of 50 mM capsaicin was prepared in 100% ethanol. The maximum concentration of ethanol in the superfusate was 0.002%, which had no apparent effects on current properties. As GTPγ-S was used as Li^+ salts, control voltage-clamp recordings were made in neurons dialyzed with 500 μM Li^+ without GTP added. The inflammatory soup was prepared daily and contained 50 nM bradykinin (BK), 500 nM prostaglandin-E2 (PGE2), 1 μM histamine (His), 500 nM norepinephrine (NE), and 2 μM ATP.

Computer Simulation of Small DRG Neurons

Simulations were performed assuming a temperature of 22°C, the temperature at which the experimental data were recorded. A single compartment simulated the DRG neuron with a passive leakage current I_{Leak} and four voltage-gated currents described by Hodgkin-Huxley kinetics (Hodgkin and Huxley, 1952): two Na^+ currents I_{SNS} and I_{NaN} through $Na_v1.8$ (SNS) and $Na_v1.9$ (NaN) channels, respectively, and two K^+ currents I_{Kdr} and I_{KM} through delayed rectifier and noninactivating M/KCNQ channels (Delmas and Brown, 2005), respectively. For each current (X = Leak, SNS, NaN, Kdr, or KM), the maximum specific conductivity $\underline{G}_X$ (per unit membrane area) was adjusted so that, in our single-compartment model with the membrane area $S = 1256.76\ \mu m^2$, the corresponding partial conductance ($\underline{G}_X \cdot S$) fitted the single-cell value obtained in experiments. When required, other values were used (see Herzog et al., 2001; Blair and Bean, 2002; Passmore et al., 2003; Coste et al., 2004, 2007). Specific membrane capacitance was $C_m = 1\ \mu F/cm^2$. Reversal potentials were: $E_L = -80$ mV for the leak current, $E_{Na} = +60$ mV for Na^+ currents, and $E_K = -80$ mV for K^+ currents. A temperature factor in the equations for voltage-dependent kinetic variables below was $Q_{10} = 3^{(t^\circ - 22)/10}$ (=1 at temperature T = 22°C). Computer simulations were performed using NEURON software (Hines and Carnevale, 2001). These provided numerical solution to the differential equations relating the current densities per unit membrane area and the transmembrane voltage E: $C_m \cdot dE/dt = -I_{Leak} - I_{SNS} - I_{NaN} - I_{Kdr} - I_{KM} - I_{stim}$, where I_{stim} is the stimulating current generated by extrinsic source. Below is the list of partial currents with corresponding parameters and equations for the kinetic variables of activation/inactivation.

Passive Leakage Current. ($\underline{G}_{Leak} = 0.261469\ mS/cm^2$, $\underline{G}_{Leak} \cdot S = 3.3$ nS): $I_{Leak} = \underline{G}_{Leak} \cdot (E - E_{Leak})$.

SNS Sodium Current. ($\underline{G}_{SNS} = 7.16218\ mS/cm^2$, $\underline{G}_{SNS} \cdot S = 90$ nS): $I_{SNS} = \underline{G}_{SNS} \cdot m \cdot h \cdot s \cdot u \cdot (E - E_{Na})$. Activation variable m is as follows: $dm/dt = (m_\infty - m)/\tau_m$; $m_\infty = 1/(1 + \exp(-(E + 20)/6.2))$; $\tau_m = \exp(-(E + 12.5)/14)/(1 + \exp(-(E + 35)/4.6))$. Fast inactivation variable h is as follows: $dh/dt = (h_\infty - h)/\tau_h$; $h_\infty = 1/(1 + \exp((E + 30.0)/7))$; $\tau_h = \exp(-(E - 10)/9.1)/(1 + \exp(-(E + 37)/2.2))$. Slow inactivation variable s is as follows: $ds/dt = (s_\infty - s)/\tau_s$; $s_\infty = 1/(1 + \exp((E + 45)/8))$; $\tau_s = 1/(\alpha_s + \beta_s)$; $\alpha_s = Q_{10} \cdot \sigma_s \cdot 5.4203/(1 + \exp((E + 79.816)/16.269))$; $\beta_s = Q_{10} \cdot \sigma_s \cdot 5.0757/(1 + \exp(-(E + 15.968)/11.542))$, where $\sigma_s = 0.001$ was the slowing factor. For the slow inactivation s of this current, the parameters of the voltage-dependent forward and backward rate constants α_s and β_s were determined with the Fitting/Parameterized Function tool of NEURON applied to the experimental data. Ultra-slow inactivation variable u is as follows: $du/dt = (u_\infty - u)/\tau_u$; $u_\infty = 1/(1 + \exp((E + 51)/8))$; $\tau_u = 1/(\alpha_u + \beta_u)$; $\alpha_u = Q_{10} \cdot \sigma_u \cdot 2.0434/(1 + \exp((E + 67.499)/19.51))$; $\beta_u = Q_{10} \cdot \sigma_u \cdot 1.9952/(1 + \exp(-(E + 30.963)/14.792))$, where $\sigma_u = 0.0002$ was the slowing factor.

NaN sodium current. ($\underline{G}_{NaN} = 2.38739\ mS/cm^2$, $\underline{G}_{NaN} \cdot S = 30$ nS): $I_{NaN} = \underline{G}_{NaN} \cdot m \cdot h \cdot s \cdot (E - E_{Na})$. Activation variable m: $dm/dt = (m_\infty - m)/\tau_m$; $m_\infty = \alpha_m \cdot \tau_m$; $\tau_m = 1/(\alpha_m + \beta_m)$; $\alpha_m = Q_{10} \cdot 0.47/(1 + \exp(-(E - V_{shift} + 28)/10.3))$; $\beta_m = Q_{10} \cdot \exp(-(E - V_{shift} + 74)/5.7)$. Fast inactivation variable h: $dh/dt = (h_\infty - h)/\tau_h$; $h_\infty = \alpha_h \cdot \tau_h$; $\tau_h = 1/(\alpha_h + \beta_h)$; $\alpha_h = Q_{10} \cdot 0.091/(1 + \exp((E - V_{shift} + 116)/18.8))$; $\beta_h = Q_{10} \cdot 0.03/(1 + \exp(-(E - V_{shift} + 40)/10))$. Slow inactivation variable s: $ds/dt = (s_\infty - s)/\tau_s$; $\tau_s = 1/(\alpha_s + \beta_s)$; $\alpha_s = Q_{10} \cdot 0.001 \cdot \exp(-(E - V_{shift} + 137)/17.5)$; $\beta_s = Q_{10} \cdot 0.002/(1 + \exp(-(E - V_{shift} + 26.0)/21.0))$, $s_\infty = 1.029/(1 + \exp((E - V_{shift} + 93)/12))$. Here setting V_{shift} parameter equal to 0 or 20 mV provided the simulated voltage-dependent kinetics that corresponded to NaN/Nav1.9 current in the presence of internal F^- or Cl^-, respectively (Coste et al., 2004).

Delayed Rectifier Potassium Current. ($\underline{G}_{Kdr} = 0.7957967\ mS/cm^2$, $\underline{G}_{Kdr} \cdot S = 10$ nS): $I_{Kdr} = \underline{G}_{Kdr} \cdot n^4 \cdot (E - E_K)$. Activation variable

n: $dn/dt = (n_\infty - n)/\tau_n$; $n_\infty = \alpha_n \cdot \tau_n$; $\tau_n = 1/(\alpha_n + \beta_n)$; $\alpha_n = Q_{10} \cdot 0.00126 \cdot (E + 14.27)/(1 - \exp(-(E + 14.27)/10))$; $\beta_n = Q_{10} \cdot 0.125 \cdot \exp(-(E + 55)/2.5)$.

M/KCNQ Potassium Current. ($\underline{G}_{KM}$ = 1.351 mS/cm^2, $\underline{G}_{KM} \cdot S$ = 2 nS) described according to the data described in Passmore et al. (2003) and our unpublished experimental data: $I_{KM} = \underline{G}_{KM} \cdot n \cdot (E - E_K)$. Activation variable n: $dn/dt = (n_\infty - n)/\tau_n$; $\tau_n = 1/(\alpha_n + \beta_n)$; $\alpha_n = Q_{10} \cdot 0.00395 \cdot \exp((E + 30)/40)$; $\beta_n = Q_{10} \cdot 0.00395 \cdot \exp(-(E + 30)/20)$; $n_\infty = 1/(1 + \exp(-(E + 30)/6))$.

Online Supplemental Material

This paper contains one supplemental figure (available at http://www.jgp.org/cgi/content/full/jgp.200709935/DC1) that shows the generation and genotyping of the Nav1.9$^{-/-}$ mice. The presence of an IRES/β-galactosidase cassette in the disrupted allele led to the expression of β-galactosidase in some small and medium diameter DRG neurons but rarely in large diameter neurons.

RESULTS

Complex Electrophysiological Behaviors of Nociceptors Expressing NaN/Nav1.9 Current

Because NaN/Nav1.9 channels give rise to a "persistent" Na^+ current at subthreshold voltages, it has been proposed to sustain subthreshold depolarizations (Herzog et al., 2001; Baker et al., 2003; Coste et al., 2004). To further examine the role of NaN/Nav1.9 current in nociceptors' excitability we studied the firing activities of small diameter (<27 μm) DRG neurons recorded using 30 mM fluoride in the pipette solution (Cummins et al., 1999; Coste et al., 2004; Maruyama et al., 2004). The presence of NaN/Nav1.9 current was first monitored in the voltage clamp mode and firing behavior was then studied in the current clamp mode (see Materials and methods). Fig. 1 A shows representative responses to current injection in a small Nav1.9$^{+/+}$ DRG neuron. These responses were typically elicited by brief current pulses in steadily hyperpolarized neurons in order to partly remove slow inactivation of NaN/Nav1.9 channels (Cummins et al., 1999; Coste et al., 2004). At subthreshold current intensities, membrane potential changes mainly reflected a passive RC membrane behavior. When the intensity was increased neurons exhibited prolonged depolarizations in response to brief pulses of depolarizing current. The responses showed signs of regenerative origin, adding to the passive electrononic response and outlasting the stimulus by significant amount of time (Fig. 1 A). Above a threshold pulse intensity, depolarizing pulses elicited plateau depolarizations and repetitive AP discharges, in an all or none manner. The duration of the plateau varied from cell to cell, ranging from 300 ms to 2 s and was the longest in cells with large NaN/Nav1.9 current. During the plateau phase, membrane potential slowly decayed from −41 ± 2 to −57 ± 1 mV (n = 17) and firing ceased before termination of the plateau. Plateau potentials terminated spontaneously with slow sigmoid-like trajectories (Fig. 1 A, arrows) and were followed by postexcitatory hyperpolarization. Such firing behaviors were observed in 22 out of 27 Nav1.9$^{+/+}$ DRG neurons. All of these cells showed NaN-mediated negative slope resistance in their *I-V* relationships (Fig. 1 A, inset). A small number of Nav1.9$^{+/+}$ neurons (n = 5/27) seemed to lack the ability to fire plateau potentials in response to current steps. When switched back to voltage-clamp mode, these cells did not show NaN/Nav1.9-dependent negative slope resistance at very negative voltages (unpublished data).

The presence of NaN/Nav1.9-mediated negative slope resistance predicts that DRG neurons possess the potential to generate bursting discharges. These predictions were tested in specific current clamp experiments in which baseline membrane potentials were adjusted by DC bias to values more negative than the unstable voltage region. At baseline V_m of approximately −95 mV, Nav1.9$^{+/+}$ DRG neurons generated spontaneous, quasi rhythmic bursts. In Fig. 1 B, the cell spontaneously moved from quiescence at hyperpolarized potentials to bursting. The cell stayed in the metastable silent state for several tens of seconds before spontaneously returning to the firing state. Provided the membrane potential was maintained without large variation, back and forth transitions between bursts and hyperpolarized silent states occurred spontaneously throughout the recording session (which lasted 42 min). With repeated bursts, plateau potentials showed very stable up state depolarization (−45 to −51 mV), constant duration (∼8 s), and regular interburst intervals (∼35 s) (Fig. 1, B and C). These spontaneous burst discharges were observed in 14 out of 21 Nav1.9$^{+/+}$ DRG neurons, which showed prominent NaN/Nav1.9 current.

In most Nav1.9$^{+/+}$ DRG neurons, burst firing coexisted with conditional bistable behavior. To exhibit bistable behavior, the *I-V* relationship must intersect the current baseline at three points. This was achieved by injecting a bias current of −50 pA in Fig. 1 D. Under this condition, the cell continued to fire slowly but could be turned off actively with brief hyperpolarizing current injection, which brought the membrane potential to very negative values in the left hand region of the *I-V* curve (Fig. 1 D, blue trace). These large hyperpolarizing responses resulted from the deactivation of persistent NaN/Nav1.9 channels. The process continued in a self-reinforcing manner until most NaN/Nav1.9 channels were completely deactivated. This gave a hyperpolarizing response its all or none behavior and sigmoidal time course (Fig. 1 E). Bistable plateauing cells could stay in the hyperpolarized state, at about −85 mV, for several seconds but could be switched on by brief hyperpolarizing current pulses. Black trace in Fig. 1 D shows that rebound excitation observed at hyperpolarizing current termination was capable to generate full blown plateau potential, thereby promoting bursts of action potentials and conditional bistable behavior.

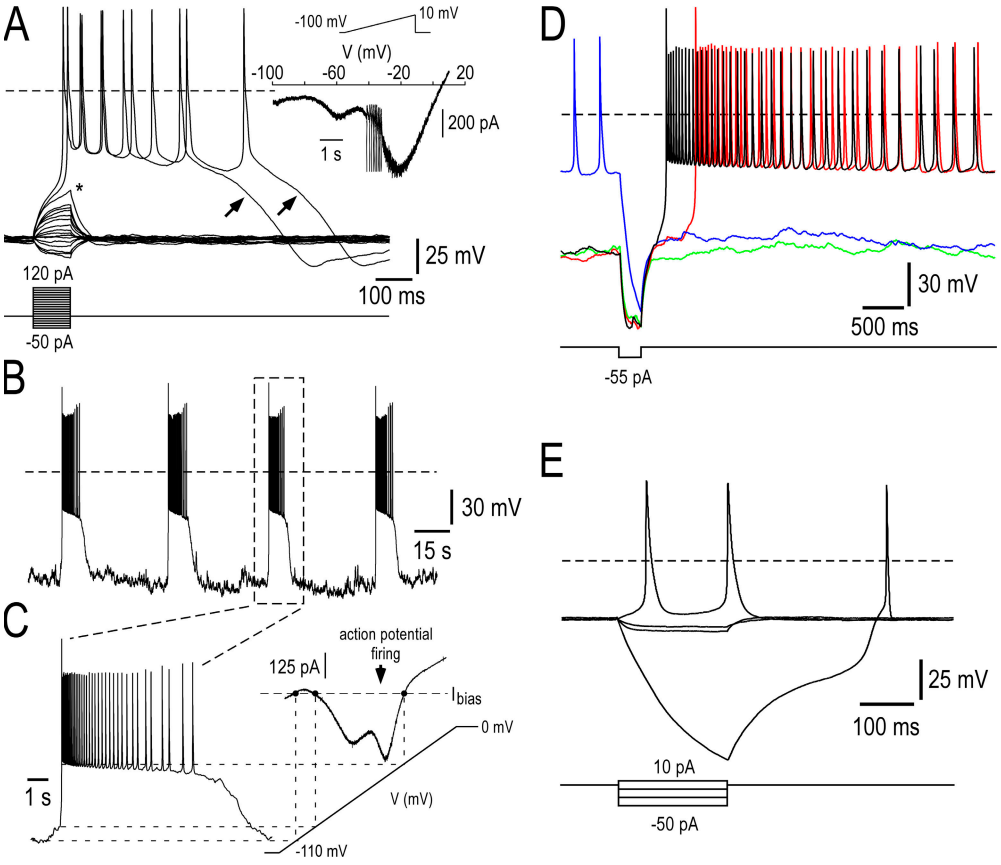

Figure 1. Self-sustained plateau depolarization, burst firing, and conditional bistable behaviors in Nav1.9$^{+/+}$ DRG neurons (A) Representative current-clamp responses of a Nav1.9$^{+/+}$ DRG neuron (25 pF) to 100 ms current pulse injection. Steady bias current (−85 pA) was injected to hyperpolarize the cell to between −87 and −92 mV. Injected current pulse was varied in amplitude with 10 pA increments. Note that low intensity pulses elicited passive RC-circuit type responses whereas above-threshold depolarizing pulses triggered self-sustained plateau depolarization and repetitive firing. The asterisk indicates threshold potential for the slow regenerative response and the arrow shows the termination of the plateau phase, which is often followed by a postexcitatory hyperpolarization. (Inset) The same cell was subjected to slow voltage ramp from −100 to +10 mV. Note the "W-shaped" *I-V* relationship. (B) Spontaneous transitions between quiescent and firing states in a Nav1.9$^{+/+}$ DRG neuron (27 pF). Application of bias current (−72 pA) revealed spontaneous bursting behavior, characterized by regenerative plateau depolarization carrying trains of action potentials and separated by silent states. (C) The time scale of the third burst in B is enlarged to illustrate the plateau depolarization and its relationship with the corresponding *I-V* curve. (D) Electrical activity recorded from a Nav1.9$^{+/+}$ DRG neuron (33 pF) in response to a 300-ms hyperpolarizing current injection (−55 pA) applied with a −50-pA bias current. Four successive sweeps, each lasting 5,318 ms, have been superimposed to show the transition between bursting activity and silent state. The neuron showed either prolonged periods of membrane depolarization carrying trains of action potentials or remained silent at ∼−85 mV. Transition between the two states was induced by applying pulse hyperpolarizations, which either deactivated the plateau-generating system or promoted rebound excitation. (E) Families of superimposed membrane potential changes evoked by a series of current pulse injection in a Nav1.9$^{+/+}$ DRG neuron (27 pF). Membrane potential was adjusted manually to between −35 and −40 mV by DC bias, immediately after conditioning V_m at −90 mV. Note that step increase in injected hyperpolarizing current caused linear response, up to a critical value at which a large active hyperpolarization occurred. Rebound depolarization followed a sigmoid-like trajectory, indicative of a metastable state. Recordings made using the intracellular solution 2 (Table I; 0 mM CsCl, 30 mM CsF, 100 mM KCl).

NaN/Nav1.9 Sustains Subthreshold Depolarization and Plateau Potentials

To measure the ionic currents flowing during plateau potential and burst discharges in DRG neurons, we used the command waveform voltage clamp technique. We first recorded bursting discharges in small DRG neurons (26 ± 4 pF; average input resistance of 1.5 ± 0.4 GΩ, $n = 17$) in which stepped voltage clamp experiments revealed the presence of both NaN/Nav1.9 and SNS/Nav1.8 currents (Fig. 2 A, left). We used short (5 ms) current injections to generate burst discharges, leaving the plateau potential free of the effect of injected current. Fig. 2 A illustrates the ion currents flowing during the prerecorded burst firing response after the amplifier was switched into the voltage clamp mode. The inward current was entirely Na^+ since it was abolished by complete substitution of Na^+ by sucrose (unpublished data). A relatively rapid TTX-R Na^+ current, possibly SNS/Nav1.8, flowed during the first action potential in the voltage command waveform, reaching maximal amplitude during the upstroke (Blair and Bean, 2002). This component of TTX-R Na^+ current strongly inactivated by the third action potential and then increased again during subsequent action potentials, likely as the result of recovery from inactivation as interspike intervals increased and plateau potential repolarized. In addition, there was a persistent component of TTX-R Na^+ current, most evident during the plateau phase at the end of the waveform as steady current of approximately −250 ± 40 pA ($n = 8$). To determine whether this persistent current was NaN/Nav1.9, the burst discharge command waveform was injected into small DRG neurons

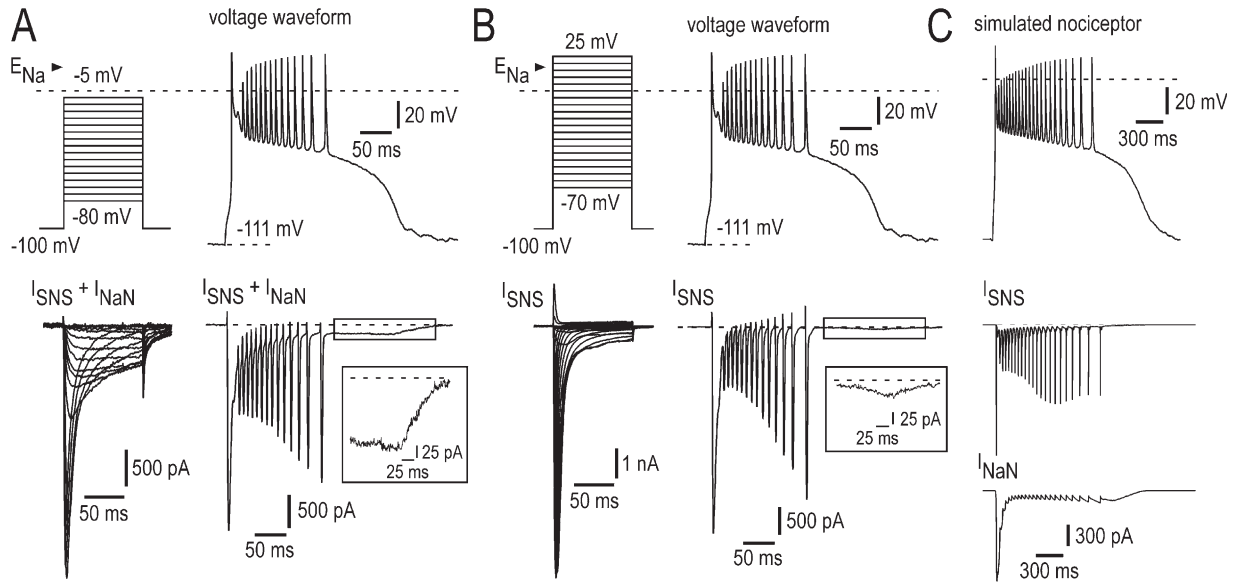

Figure 2. NaN/Nav1.9 current is flowing during the long-lasting depolarization plateau. (A, top) Voltage command taken from current clamp experiment in a small DRG neuron (28 pF) expressing both SNS/Nav1.8 and NaN/Nav1.9 in response to a short depolarizing stimulus (+85 pA, 5 ms, not depicted) and further used as a voltage command clamping the neuron. (bottom) Total inward current elicited during the long-lasting depolarization plateau and discharge waveform (right) or stepped protocol (left) in the same cell. The inset shows the steady TTX-R Na^+ current (putative NaN/Nav1.9) flowing during the plateau phase. $[Na^+]_o$ = 60 mM. (B, top) The voltage command waveform as in A was injected into a small DRG neuron (32 pF) that expresses SNS/Nav1.8 but not NaN/Nav1.9. (bottom) SNS/Nav1.8 current elicited during the long-lasting depolarization plateau and discharge waveform (right) or the stepped protocol (left). $[Na^+]_o$ = 60 mM. The inset shows the weak activation of SNS/Nav1.8 during the plateau phase. (C) Dynamic clamp test of partial currents in a simulated small DRG neuron containing NaN/Nav1.9, SNS/Nav1.8, M/KCNQ, KDr, and leak conductances (see Materials and methods for further details) commanded by a long-lasting depolarization plateau waveform. (bottom) Simultaneous SNS/Nav1.8 and NaN/Nav1.9 currents generated in the simulated DRG neuron during dynamic clamp with the voltage command waveform. E_{Na} = +60 mV. Recordings in A and B made using the intracellular solution 1 (Table I; 100 mM CsCl, 30 mM CsF, 0 mM KCl).

lacking NaN/Nav1.9 but expressing SNS/Nav1.8 (n = 8). Records from one such cell is shown in Fig. 2 B. SNS/Nav1.8 reached its maximum during the early phases of the burst firing waveform, inactivated by the time of the stronger depolarization during the plateau phase and recovered when plateau potential had repolarized to near −50 mV. The persistent current was always near zero during the late plateau phase (−27 ± 7 pA, Fig. 2 B, inset), suggesting that action potential was contributed by SNS/Nav1.8 and plateau potential by NaN/Nav1.9.

To further gain insight into the membrane dynamics responsible for plateau potential and bursting, we ran computational simulations of small DRG neurons. The passive properties used for the model were chosen to approximate the input resistance and membrane time constant observed experimentally. In this version of the model, five conductances were employed: the leak conductance, SNS/Nav1.8, NaN/Nav1.9, the voltage-gated KCNQ2/3 (Kv7), and the voltage-gated outwardly rectifying K^+ conductance (IKDr). The parameters for these ionic conductances were chosen to approximate the properties of these currents in small DRG neurons (see Materials and methods). In the model, the response to the 5-ms depolarizing stimulus, which is subthreshold for action potential generation in the absence of NaN/Nav1.9, triggered a subthreshold regenerative depolarization and action potential followed by a plateau potential triggering spikes as observed experimentally (Fig. 2 C). Plots of individual transmembrane currents in Fig. 2 C revealed the mechanism of the plateau potential in this model. NaN/Nav1.9 current did not contribute substantially to the generation of action potentials during burst firing but was temporally associated with subthreshold depolarization triggering first action potential and plateau generation. Conversely, SNS/Nav1.8 was responsible for the surge of I_{Na} that occurs during the rising phase of action potentials but had only minor implication in the later phase of the plateau depolarization.

Firing Patterns in Small DRG Neurons from Nav1.9$^{-/-}$ Mice

Gene targeting strategy was used to disrupt the *Scn11a* gene coding for the Nav1.9 channel α subunit (Fig. S1, available at http://www.jgp.org/cgi/content/full/jgp.200709935/DC1). TTX-R Na^+ currents were studied by using reduced driving force for Na^+ ($[Na^+]_o$ = 60 mM) and an internal solution containing ATP and GTP to ensure stable recordings. We isolated TTX-R Na^+ currents from T-type Ca^{2+} currents with 1 mM amiloride and 5 μM

La^{3+}, which caused minimal alteration in NaN biophysical properties (Coste et al., 2007). Under these conditions, NaN current could be recorded in isolation from low-threshold Ca^{2+} currents and the neurons were amenable to careful voltage-clamp. With TTX (500 nM) in the bathing solution, depolarizing pulses from a holding potential of −100 mV evoked NaN currents in the majority of small DRG neurons recorded with internal F^- (30 mM CsF; see Cummins et al., 1999; Coste et al., 2007).

Voltage-clamp experiments were performed in small Nav1.9$^{+/+}$ and Nav1.9$^{-/-}$ DRG neurons having a mean C_m of 28.2 ± 1.3 pF (n = 26) and 30.5 ± 2.8 pF (n = 18), respectively. NaN currents were evoked by depolarizing voltage pulses in 21 out 26 Nav1.9$^{+/+}$ DRG neurons tested (Fig. 3 A). The NaN current was characterized by its low threshold of activation (−75 ± 1 mV; n = 21) and slow kinetics of activation and inactivation (Fig. 3 A). By contrast, NaN currents were not detected in Nav1.9$^{-/-}$ DRG neurons (n = 18/18; Fig. 3, B, C, and E). Inward current density at −60 mV averaged −22 ± 3.2 pA/pF in Nav1.9$^{+/+}$ neurons (n = 20) but was only −0.3 ± 0.1 pA/pF in Nav1.9$^{-/-}$ neurons (n = 18, Fig. 3 C). SNS/Nav1.8 current, which is distinguishable from NaN current by its more positive activation threshold and faster kinetics, was seen in most NaN-expressing DRG neurons (n = 20/21). Both currents could be recorded under good voltage clamp conditions using relatively slow voltage ramp commands. The negative slope regions associated with NaN and SNS/Nav1.8 currents gave the ramp-induced *I-V* relationship a "W shape" (Fig. 3 D, red trace). Conditioning membrane potential to −50 mV for several seconds, before ramp application fully inactivated NaN current, left the inward current attributable to SNS/Nav1.8 mostly unchanged (Fig. 3 D, black trace). By doing so, we compared properties of SNS/Nav1.8 currents in Nav1.9$^{+/+}$ and Nav1.9$^{-/-}$ neurons. Activation threshold of SNS/Nav1.8 in Nav1.9$^{-/-}$ neurons was −54.4 ± 1.7 mV (n = 18), which was not significantly different from that in Nav1.9$^{+/+}$ neurons (Fig. 3, E and F).

To test how the loss of Nav1.9 subunits affects nociceptors' excitability, we recorded firing patterns of small Nav1.9$^{-/-}$ DRG neurons (Fig. 4). Nav1.9$^{-/-}$ neurons responded to brief above threshold depolarizing currents with firing of action potentials and slow after depolarizing potentials that did slightly outlast the current step (Fig. 4 A, arrow). However, Nav1.9$^{-/-}$ DRG neurons were no longer capable to generate plateau depolarization (n = 19). In addition, small Nav1.9$^{-/-}$ neurons did not show intrinsic bursting behavior (n = 18) (Fig. 4 B). Indeed, when the membrane potential was adjusted to hyperpolarized levels by DC bias no spontaneous bursting activity could be revealed, and cells remained quiescent. These cells, however, responded to brief above threshold depolarizing currents with firing of action potentials (Fig. 4 B). The injection of hyperpolarizing currents gave graded exponential responses in Nav1.9$^{-/-}$ DRG neurons (Fig. 4 C), which differed from the "all or none" behavior of active hyperpolarizing responses observed in Nav1.9$^{+/+}$ DRG neurons (compare with Fig. 1 E).

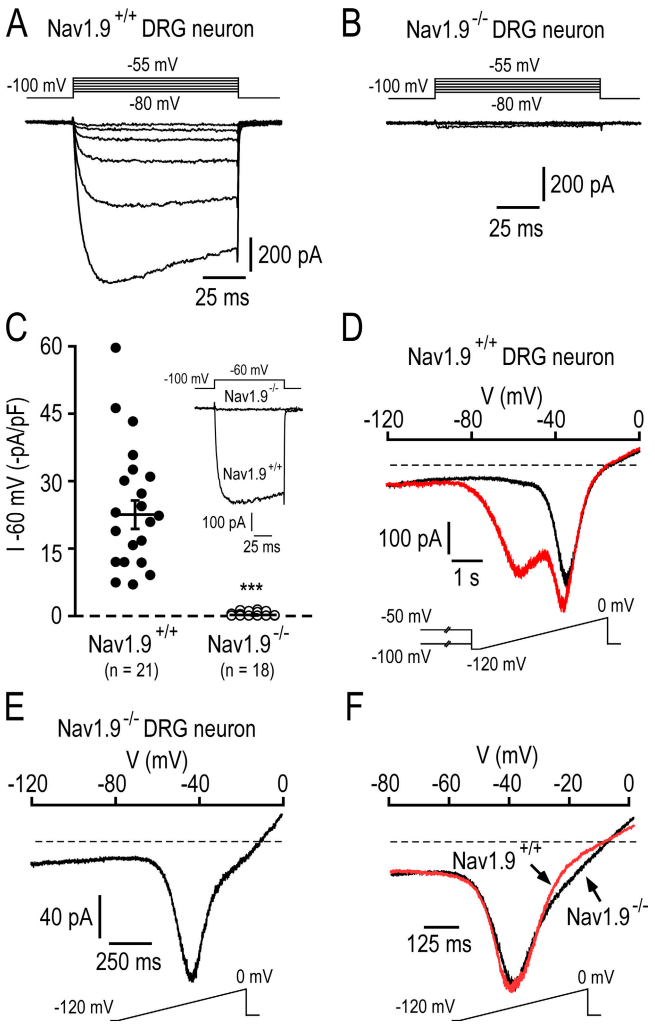

Figure 3. Properties of TTX-R Na^+ currents in Nav1.9$^{-/-}$ DRG neurons. Families of current traces elicited in a 33 pF Nav1.9$^{+/+}$ DRG neuron (A) and a 29 pF Nav1.9$^{-/-}$ DRG neuron (B). Currents were evoked by 100-ms depolarizing voltage steps from −80 to −55 mV in 5-mV increments from a holding potential of −100 mV. (C) Scatterplot showing the amplitude of the TTX-R Na^+ current recorded at −60 mV in small Nav1.9$^{+/+}$ and Nav1.9$^{-/-}$ DRG neurons. The bars indicated the mean amplitude ± SEM. ***, $P < 0.001$. (Inset) examples of currents evoked at −60 mV in two representative Nav1.9$^{+/+}$ and Nav1.9$^{-/-}$ neurons. (D) Whole-cell currents elicited in the Nav1.9$^{+/+}$ neuron shown in A by a 8-s ramp depolarization from −120 to 0 mV (rate, 15 mV s^{-1}), after 30-s conditioning at −100 mV (red trace) or −50 mV (black trace). (E) SNS currents elicited by a 1.6-s ramp depolarization from −120 to 0 mV (rate, 75 mV s^{-1}) in the Nav1.9$^{-/-}$ neuron shown in B. (F) Comparison of ramp-activated SNS currents in Nav1.9$^{+/+}$ (red trace) and Nav1.9$^{-/-}$ (black trace) DRG neurons. Each trace is the average of four different cells, and currents were normalized to facilitate comparison. Ramps were applied from −120 to 0 mV at a rate of 75 mV s^{-1}. In Nav1.9$^{+/+}$ neurons, SNS currents were isolated from NaN currents as in D. Recordings made using the intracellular solution 1 (Table I; 100 mM CsCl, 30 mM CsF, 0 mM KCl).

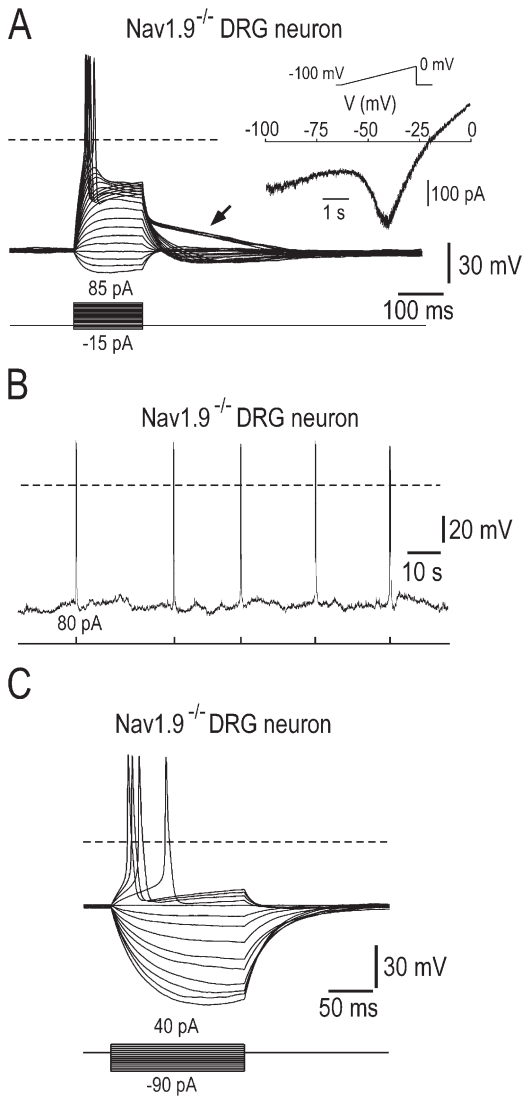

Figure 4. Loss of self-sustained plateau depolarization, burst firing, and conditional bistable behaviors in Nav1.9$^{-/-}$ DRG neurons. (A) Family of superimposed membrane potential changes evoked by a series of 150-ms current pulse injection in a Nav1.9$^{-/-}$ DRG neuron (22 pF). Low-intensity pulses evoked passive responses whereas large stimuli evoked action potentials and slow afterdepolarization potentials that outlasted the stimulus (arrow). Injected current was varied in amplitude with 5-pA increments. (Inset) The same cell was subjected to slow voltage ramp from −100 to 0 mV. Note the "N-shaped" *I-V* relationship (compare with Fig. 1 C). (B) Lack of spontaneous activity in a Nav1.9$^{-/-}$ DRG neuron (31 pF) held at ∼−85 mV (bias current, −35 pA). The cell was challenged by 100-ms depolarizing step currents and responded by short spike volleys. (C) Families of superimposed membrane potential changes evoked by a series of current pulse injection in a Nav1.9$^{-/-}$ DRG neuron (31 pF). Membrane potential was adjusted manually to between −35 and −40 mV by DC bias, immediately after conditioning V_m at −90 mV. Note that current pulses evoked responses with exponential on and off trajectories indicating a passive RC membrane behavior (compare with Fig. 1 E). Recordings made using the intracellular solution 2 (Table I; 0 mM CsCl, 30 mM CsF, 100 mM KCl).

As a consequence, none of the Nav1.9$^{-/-}$ DRG neurons recorded displayed bistable behaviors (n = 18).

Inflammatory Mediators Applied Singly Failed to Increase Nav1.9 Channel Activity

The ability of NaN/Nav1.9 current to underlie subthreshold regenerative responses relies on its upregulation by internal fluoride (Cummins et al., 1999; Coste et al., 2004). To test the idea that upregulation of NaN/Nav1.9 current might be a mechanism for inflammatory mediator–induced hyperalgesia (Priest et al., 2005; Amaya et al., 2006), we investigated whether inflammatory mediators modulate NaN/Nav1.9 current.

In this set of experiments, internal CsF was substituted by CsCl, and ATP (4 mM) and GTP (500 μM) were still present in the pipette solution. Five different mediators, bradykinin (BK, 1–5 μM), prostaglandin E2 (PGE2, 2 μM), histamine (His, 500 μM), norepinephrine (NE, 100 μM), and ATP (100–250 μM) were tested on TTX-R Na^+ currents recorded at −50 mV, a potential at which SNS/Nav1.8 is small or absent (Coste et al., 2007). Fig. 5 A shows representative TTX-R Na^+ current traces recorded before and during exposure to BK (1 μM) and PGE2 (2 μM). BK and PGE2 had no significant effect either on NaN/Nav1.9 currents recorded at −50 mV (n = 8–13) (Fig. 5, A and B) or *I-V* relationships of total TTX-R Na^+ currents (not depicted). Increasing their concentrations to 5 and 10 μM, respectively, did not produce significant effect either. We confirmed that BK and PGE2 receptors were functional under our recording conditions since both BK (1 μM) and PGE2 (2 μM, not depicted) potentiated capsaicin-activated TRPV1 current in small DRG neurons (Fig. 5 C). Likewise, histamine, ATP, and NE each used at high concentrations failed to upregulate the NaN/Nav1.9 current (n = 6–8) (Fig. 5 B). In contrast, inclusion of GTPγ-S (500 μM, GTP omitted), a nonhydrolyzable analogue of GTP, in the patch pipette solution increased 6.7-fold NaN/Nav1.9 current from −1.78 ± 0.4 to −12 ± 2.1 pA/pF within 15 min (n = 10) (Fig. 5, A and B). In control experiments with GTP (500 μM) instead of GTPγ-S, NaN/Nav1.9 current amplitude remained small (−1.25 ± 0.28 pA/pF at −50 mV, n = 12) and relatively stable over 30-min recording (Fig. 5 B, inset).

The Combined Action of Multiple Inflammatory Mediators Is Required to Potentiate Nav1.9 Current

We tested whether the aforementioned mediators (e.g., BK, PGE2, His, NE, and ATP) applied concurrently, but at lower concentrations, would enhance NaN/Nav1.9 current. After exposure to the inflammatory soup, NaN/Nav1.9 underwent a 6.2-fold increase in amplitude from −1.88 ± 0.5 to −11.7 ± 1.8 pA/pF (n = 8) as measured at −50 mV (Fig. 5, A and B). The average time constant of inflammatory soup-induced NaN/Nav1.9 potentiation was 3 min (Fig. 5 B, inset), which was approximately

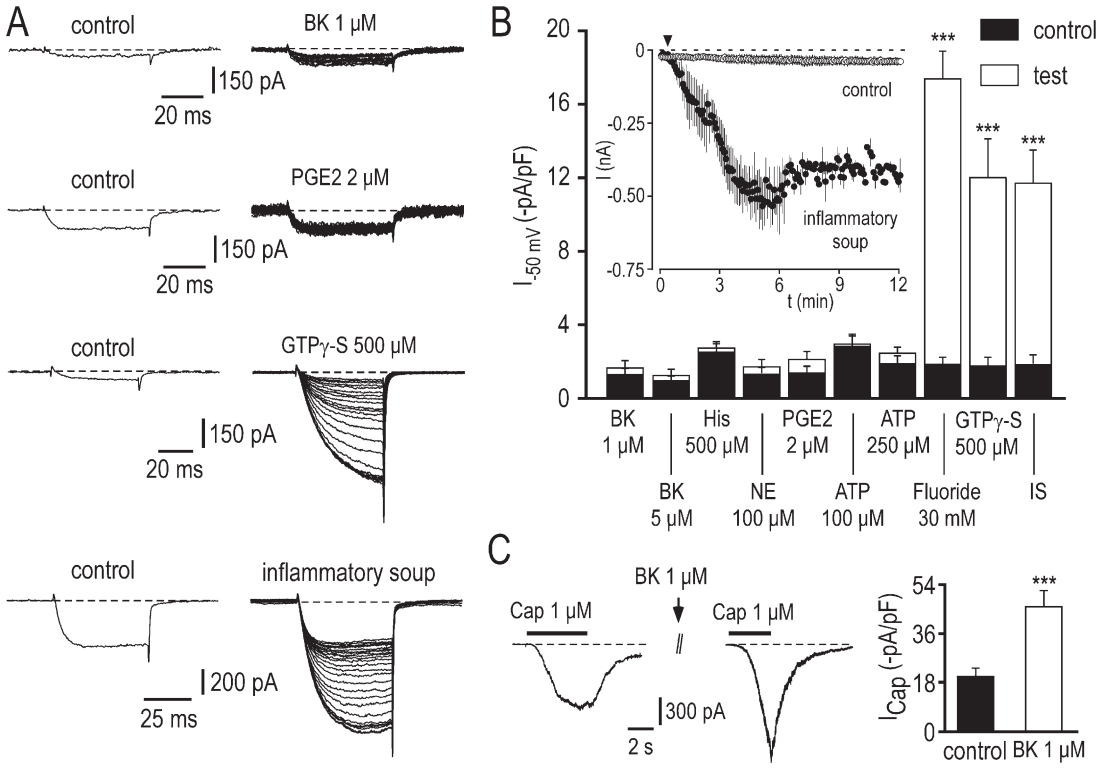

Figure 5. Inflammatory soup, but not singly applied inflammatory mediators, potentiates the NaN/Nav1.9 current. (A) Effects of BK (1 μM), PGE2 (2 μM), GTPγ-S (500 μM), and inflammatory soup (50 nM BK, 500 nM PGE2, 1 μM His, 500 nM NE, 2 μM ATP) on TTX-R Na^+ currents evoked by 50-ms depolarizing voltage steps from −100 to −50 mV. Control recordings on the left represent the average of three consecutive sweeps recorded either 2 min after patch rupturing (GTPγ-S) or immediately before drug application (e.g., BK, PGE2, and inflammatory soup). (right) Currents were evoked every 5 s. For clarity sake, only one sweep every 10 s (BK, PGE2, and inflammatory soup, 26 sweeps) or 25 s (GTPγ-S, 23 sweeps) is shown. (B) Mean NaN/Nav1.9 currents evoked at −50 mV before (black bar) and after (white bar) exposure to mediators or inflammatory soup (IS), as indicated. For comparison, increase in NaN/Nav1.9 induced by dialysis of fluoride or GTPγ-S is also shown. ***, $P < 0.001$, paired *t* test. The inset compares averaged time course of NaN/Nav1.9 current in neurons exposed (filled circles, $n = 7$) or not (open circles, $n = 12$) to the inflammatory soup. Currents were evoked as in A. The arrow indicates the start of the application of the inflammatory soup. (C) Potentiation of the capsaicin-induced TRPV1 inward current recorded at −80 mV by 1 μM BK. ***, $P < 0.001$, paired *t* test. Recordings made using the intracellular solution 3 (Table I; 130 mM CsCl, 0 mM CsF, 0 mM KCl).

twofold faster than the effects of GTPγ-S. The effects of the inflammatory soup were occluded after fluoride and GTPγ-S had reached their maximum effects (unpublished data).

The *I-V* relationships for TTX-R peak Na^+ currents in neurons undergoing NaN/Nav1.9 upregulation after intracellular dialysis of GTPγ-S or exposure to inflammatory soup are presented in Fig. 6. To better identify NaN/Nav1.9 and SNS/Nav1.8 components, current amplitude was determined both at peak and isochronally 95 ms after the onset of the test step, where the "persistent" NaN/Nav1.9 current predominates. Using this procedure, it was apparent that the increase in the overall TTX-R Na^+ current seen with GTPγ-S or the inflammatory soup resulted almost entirely from the potentiation of NaN/Nav1.9 with very little, if any, modulation of SNS/Nav1.8 current (Fig. 6, A–D). Potentiated currents extracted by subtracting control TTX-R Na^+ currents from modulated TTX-R Na^+ currents had relatively negative threshold of activation (−64 ± 1.5 mV) and slow kinetics of activation and inactivation, typical of NaN/Nav1.9. The normalized conductance of NaN/Nav1.9 currents isolated by subtraction was plotted against voltage in Fig. 6 E. Inflammatory soup-potentiated NaN/Nav1.9 exhibited voltage dependence for activation ($V_{1/2} = -44.5 \pm 2$ mV, $n = 6$) similar to value ($V_{1/2} = -47 \pm 1.5$ mV, $n = 10$; $P > 0.05$) of GTPγ-S–activated NaN/Nav1.9 current, but slightly less negative than that ($V_{1/2} = -53 \pm 1$ mV, $n = 14$; $P < 0.05$) of fluoride-enhanced NaN/Nav1.9 current.

Inflammatory Soup–Increased Excitability of Nociceptors Requires Potentiation of Nav1.9 Current

Next, we assessed whether inflammatory soup potentiation of NaN/Nav1.9 could alter excitability of small DRG neurons. Fig. 7 shows the result of a representative current clamp experiment in a neuron in which a low intensity depolarizing pulse produced only a subthreshold depolarization under control conditions. Consecutive recording segments in Fig. 7 (A–E) show that exposure to the inflammatory soup lowered the threshold for

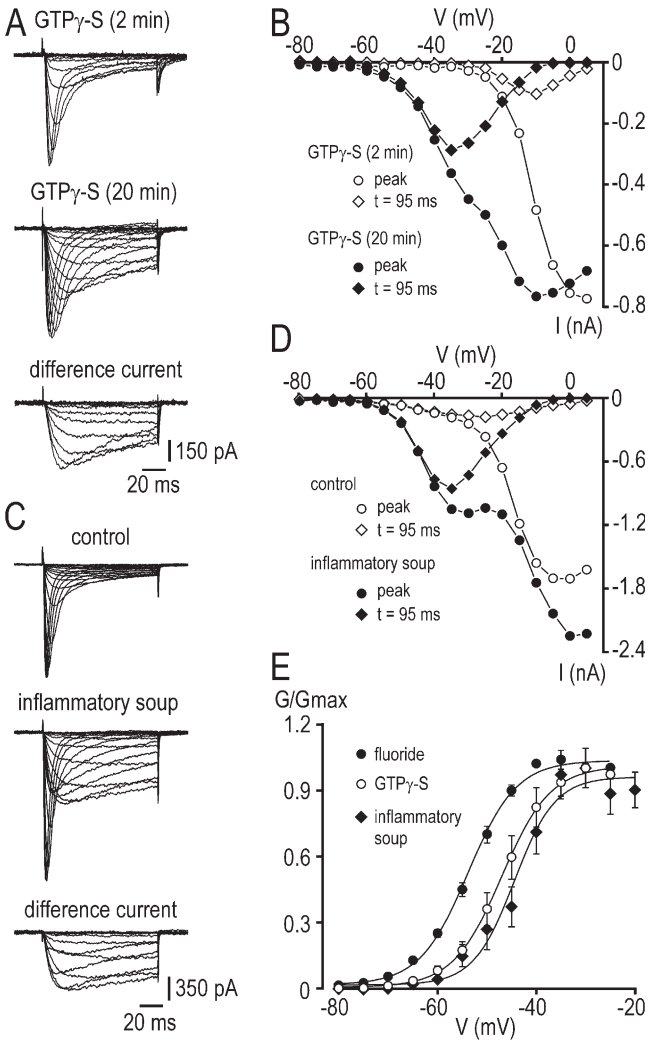

Figure 6. Voltage-dependent properties of TTX-R Na^+ currents induced by GTPγ-S and inflammatory soup in small DRG neurons. (A) Families of current traces evoked by 100-ms depolarizing voltage steps from -80 to +5 mV in 5-mV increments from −100 mV, 2 and 20 min after achieving the whole cell recording mode with internal GTPγ-S (500 μM). Difference current traces are shown for test potentials from −80 to −15 mV. (B) Current–voltage relationship of the experiment shown in A. TTX-R Na^+ currents were measured either at the peak (circles) or 95 ms after the onset of the test pulse (diamonds). (C) Families of current traces evoked by 100-ms depolarizing voltage steps from −80 to −5 mV in 5-mV increments from −100 mV, before and 5 min after exposure to the inflammatory soup (50 nM BK, 500 nM PGE2, 1 μM His, 500 nM NE, 2 μM ATP). Difference current traces are shown for test potentials from −80 to −15 mV. (D) Current–voltage relationship of the experiment shown in C. TTX-R Na^+ currents were measured either at the peak (circles) or 95 ms after the onset of the test pulse (diamonds). (E) Steady-state activation of NaN/Nav1.9 after fluoride (filled circles), GTPγ-S (open circles), and inflammatory soup (filled diamonds) had reached their maximum effects. Currents were studied using standard pulse protocol as in A and C. $V_{1/2}$ and k values were −44.5 ± 2 mV and 5.1 ± 0.5 mV (n = 6), −47 ± 1.5 mV and 5.3 ± 0.5 mV (n = 10), and −53 ± 1 mV and 5 ± 0.4 mV (n = 14) for the inflammatory soup, GTPγ-S, and fluoride conditions, respectively. Recordings made using the intracellular solution 3 (Table I; 130 mM CsCl, 0 mM CsF, 0 mM KCl).

excitability, which was associated with the occurrence of subthreshold depolarization, plateau potential with increasing height and width and firing (Fig. 7 F). Out of the 14 small DRG neurons tested with such procedure, 11 showed lowered threshold for excitability and fired either a single spike or a burst on the top of the plateau phase. By repeatedly estimating the size of NaN/Nav1.9, we found that the increase in excitability was associated with upregulated NaN/Nav1.9 (Fig. 7 G). The role of NaN/Nav1.9 in the inflammatory soup-induced nociceptor hyperexcitability was confirmed in small $Nav1.9^{-/-}$ DRG neurons. None of the $Nav1.9^{-/-}$ neurons tested (n = 8) displayed increased excitability in response to exposure to the inflammatory soup (Fig. 7 H).

Nav1.9 Current-mediated Increase in Excitability under Physiological Recording Conditions

We examined the effects of the inflammatory soup on small DRG neurons recorded with a KCl-based pipette solution and a standard external Krebs solution (no drugs added) (Fig. 8). Bath application of the inflammatory soup lowered the threshold of excitability and increased the number of action potentials in response to injected currents in 45% (n = 12) of $Nav1.9^{+/+}$ neurons tested (Fig. 8 A). The increased excitability was associated with the appearance of a nonlinear region in the subthreshold voltage range and with a reduction in the latency to the first spike, suggesting that NaN/Nav1.9 current that dominates the latency to first spike was potentiated (Fig. 8 B). Switching to the voltage clamp mode confirmed that the inflammatory soup potentiated the NaN/Nav1.9 current but also inhibited a "persistent," possibly M/KCNQ, potassium current (Fig. 8 C). These two combined actions were observed in all neurons responding to the inflammatory soup. No signs of change in the latency to the first spike and excitability were seen in $Nav1.9^{-/-}$ neurons in response to exposure to the inflammatory soup (n = 11, unpublished data).

DISCUSSION

In the present study, we demonstrated that Nav1.9 subunits are associated to the low-threshold TTX-resistant Na^+ current, first described by Cummins et al. (1999) and called NaN. The biophysical properties of the current carried by Nav1.9 have been uncertain, because its expression in heterologous systems has not been successful and because it has not been possible to reliably separate NaN and Nav1.8/SNS currents using standard pipette solution (Cummins et al., 1999; Coste et al., 2004; Maruyama et al., 2004). Here we used 30 mM internal fluoride in the patch pipette solution in order to unambigously identify neurons expressing NaN (Rugiero et al., 2003; Coste et al., 2004). Under these conditions, NaN current in mouse DRG neurons had an

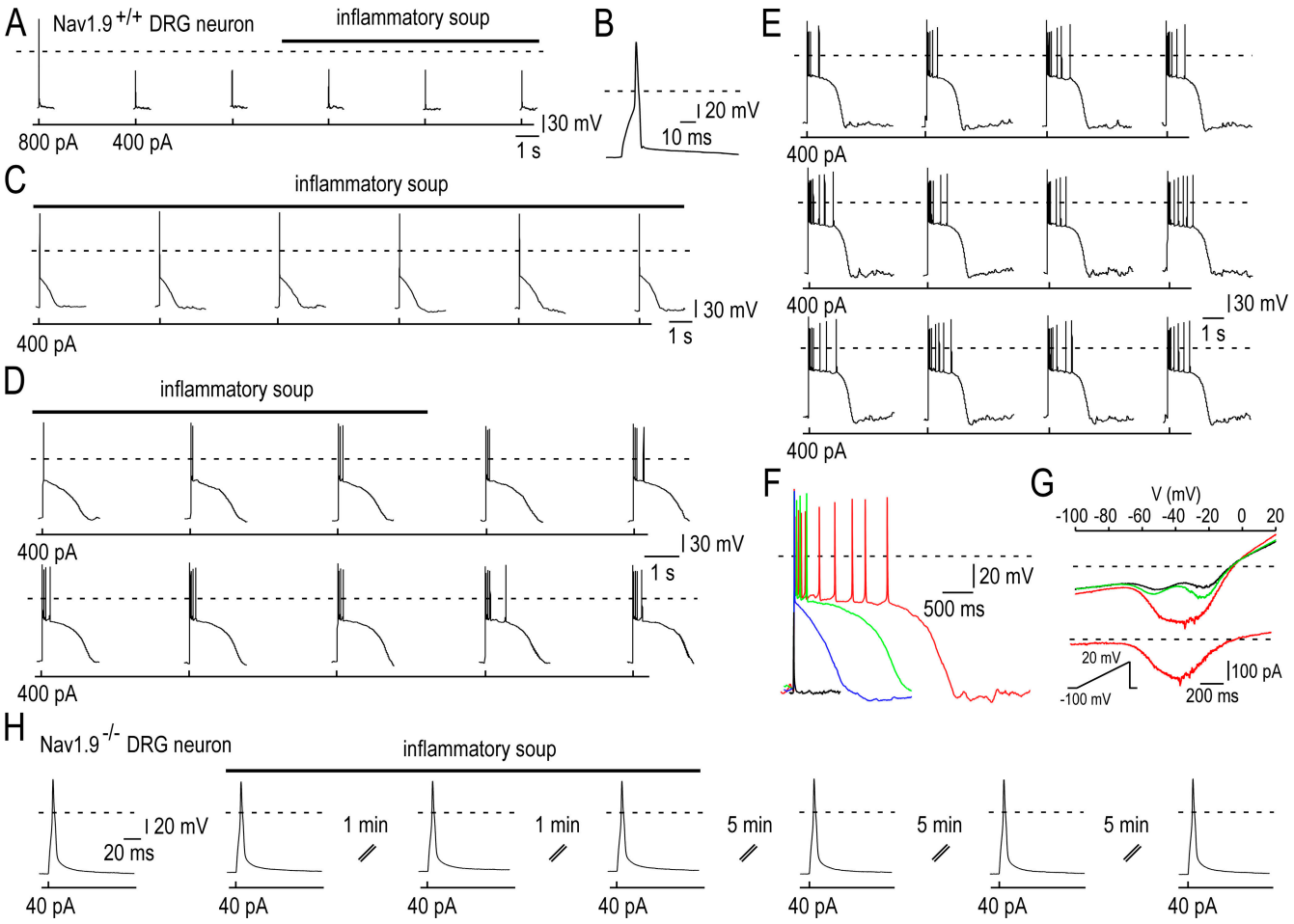

Figure 7. Inflammatory soup potentiates NaN/Nav1.9 and lowers the threshold of excitability. (A) Current-clamp responses of a Nav1.9$^{+/+}$ DRG neuron (29 pF) to 3 ms above threshold depolarizing pulse (+800 pA) or 3 ms low intensity depolarizing pulse (+400 pA). (B) Action potential triggered by the above threshold depolarizing pulse in A is shown on an expanded time scale. (C–E) Consecutive segments elapsed by 10 s showing that the subthreshold stimulus elicited action potentials, long-lasting plateau depolarization, and bursts after the addition of the inflammatory soup. The horizontal bar indicates the time and duration of application of the inflammatory soup. (F) Superimposed current-clamp responses to the subthreshold depolarizing currents shown in A (black), C (blue), D (green), and E (red). Note the increase in height and width of the plateau depolarization induced by the inflammatory soup. (G) Quasi steady-state *I-V* relationships determined by slow voltage ramps (30 mV s^{-1}) before (black), during (red), and after (green, 20 min washout) the application of the inflammatory soup. (bottom) The inflammatory soup–induced TTX-R Na^+ current obtained by subtraction displays a threshold of activation of ∼−65 mV. (H) Current-clamp responses of a Nav1.9$^{-/-}$ DRG neuron (21 pF) to 3 ms above threshold depolarizing pulse (+40 pA) before, during, and after the application of the inflammatory soup. Recordings made using the intracellular solution 4 (Table I; 30 mM CsCl, 0 mM CsF, 100 mM KCl).

activation threshold of ∼−75 mV, 20–30 mV more negative than SNS/Nav1.8 threshold, showed persistent kinetics at negative test potentials, robust slow inactivation, and fast deactivation kinetics (Coste et al., 2007). These properties are consistent with NaN previously characterized in rat and mouse DRG nociceptors (Cummins et al., 1999; Dib-Hajj et al., 2002). Because, Nav1.9$^{-/-}$ DRG neurons did not exhibit detectable NaN current relative to wild-type neurons, the present experiments demonstrate that Nav1.9 is the molecular correlate of NaN in DRG nociceptors. This is in agreement with recent studies showing that DRG neurons from mice with disrupted *Scn11a* gene have reduced persistent TTX-R Na^+ currents (Priest et al., 2005; Amaya et al., 2006), although a detailed characterization of the different TTX-R Na^+ current components was lacking.

Using Cl^- as the major internal anion, NaN/Nav1.9 channels are thought to be mostly silent in DRG neurons (Priest et al., 2005; Amaya et al., 2006), and when detected, NaN/Nav1.9 current is generally of small amplitude and exhibits a relatively positive voltage dependence (Coste et al., 2004; Maruyama et al., 2004). Internal fluoride was therefore required in our routine experiments for a better visualization of the NaN/Nav1.9 current and for probing its electrophysiological impact. Under these conditions, we demonstrated that NaN/Nav1.9 can sustain a large repertoire of firing patterns, including regenerative responses to subthreshold

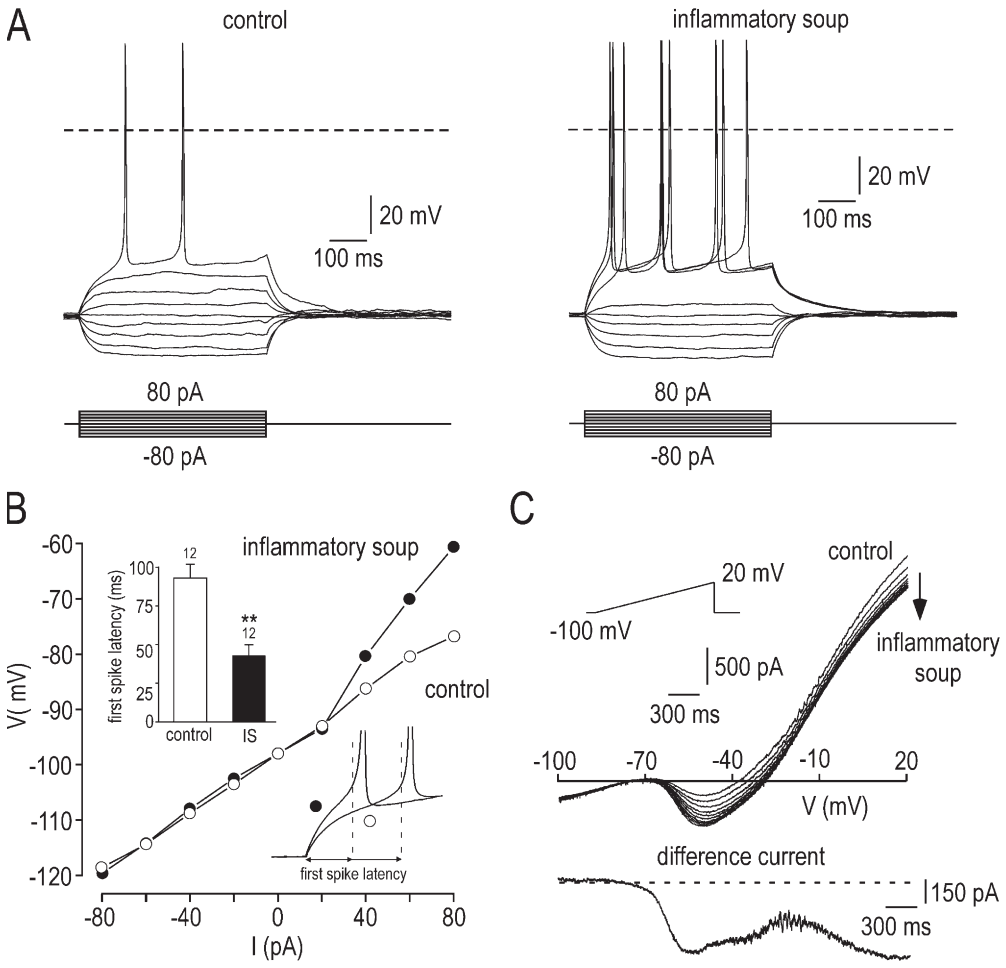

Figure 8. Inflammatory soup potentiates NaN/Nav1.9 current and lowers the threshold of excitability using a KCl-based intracellular solution. (A) Families of superimposed membrane potential changes evoked by a series of current pulse injection in Nav1.9$^{+/+}$ neuron before (left) and 3 min after the application of inflammatory soup (right). (B) Membrane potential values (collected isochronally 60 ms after the onset) plotted as a function of injected currents from the experiment shown in A. Note that injected current caused linear responses in control condition (open circle) and active depolarization in the presence of the inflammatory soup (filled circle). (right inset) Expanded traces from A showing the reduced first spike latency in the presence of the inflammatory soup (filled circle). (left inset) Mean first spike latency before (93 ± 9 ms) and during (43 ± 7 ms) the superfusion of inflammatory soup (n = 12; **, P < 0.01 paired t test). (C) Whole-cell currents elicited in the Nav1.9$^{+/+}$ neuron shown in A by a 3.3-s ramp depolarization from −100 to 20 mV (rate, 36 mV s^{-1}) before and during the superfusion of the inflammatory soup (one trace every 10 s). The bottom panel shows the inflammatory soup–induced current obtained by subtraction. Note that inflammatory soup potentiates the NaN/Nav1.9 current and inhibits an outward potassium current. Recordings made using the intracellular solution 5 (Table I; 0 mM CsCl, 0 mM CsF, 130 mM KCl).

depolarizing inputs, plateau potentials, active hyperpolarizing responses, oscillatory bursting discharges, and bistability. Thus, our data confirm and extend previous studies (Herzog et al., 2001; Renganathan et al., 2001; Coste et al., 2004; Baker, 2005; Matsutomi et al., 2006).

The ability of NaN/Nav1.9 to underlie such rich behaviors follows from the negative slope resistance in the neuron's *I-V* curve. Bursting behavior is possible when either intrinsic currents or bias current shift the negative slope resistance to lie in the region of net inward current. In this case, the *I-V* curve intersects the zero-current axis once with positive slope at potentials more positive than SNS/Nav1.8 spike threshold, enabling the neuron to initiate the plateau phase and firing without need of a stimulus. In Nav1.9$^{-/-}$ neurons, the negative slope resistance was absent, and a subthreshold zero current point was established. Consequently, plateau depolarization and burst discharges were not observed, and injected current failed to reveal any substantial subthreshold conductances that might trigger plateau potentials.

Our computer simulation provides additional evidence that bursting behavior arises from NaN/Nav1.9-depolarizing envelopes that reach a plateau at membrane potentials in between −50 and −40 mV. The "persistent" activity of NaN/Nav1.9 channels at these potentials makes them suitable to sustain the plateau phase. However, the effectiveness of NaN/Nav1.9 in promoting and maintaining plateau potentials will depend on its interaction with other currents. In particular, we provided evidence to suggest that SNS/Nav1.8, besides its role as action potential-generating system, also generates steady current, which opposes repolarization and possibly helps maintain plateau potentials. The slow inactivation of NaN/Nav1.9 channels, in conjunction with the activation of K^+ currents (IK_M, unpublished data), is likely to be responsible for the slow decay of the plateau phase and for cessation of firing, whereas termination of plateau potentials results from the voltage-dependent and self-reinforcing turning off of NaN/Nav1.9 channels. In addition, Na^+ influx via noninactivating Na^+

channels may also lead to an increase in activity of the Na^+/K^+ ATPase that in turn exerts a hyperpolarizing influence, often apparent in our recordings as a post-plateau hyperpolarization (Bostock and Grafe, 1985; Stys et al., 1993). The same cocktail of mechanisms may also contribute to maintaining the burst recurrence or the rhythmic recurrence of bursts. Collectively, these results lead to the prediction that NaN/Nav1.9 voltage-dependent kinetics, in conjunction with other currents, may control the "refractoriness" and discharge regularity of bursts in nociceptors. Future experiments will be needed to test these predictions.

It could be argued that the presence of fluoride may not be relevant to the physiological significance of NaN/Nav1.9. Therefore, we were interested in determining whether NaN/Nav1.9 enhancement could be demonstrated in DRG neurons during inflammatory challenges, particularly in light of a very recent report suggesting that NaN/Nav1.9 was insensitive to PGE2 (Zheng et al., 2007). In the experiments described here, we observed substantial upregulation of NaN/Nav1.9 after intracellular dialysis of GTPγ-S (see also Baker et al., 2003) or exposure to a cocktail of inflammatory mediators. Our results demonstrate that the concerted action of inflammatory mediators is necessary to potentiate NaN/Nav1.9 in nociceptors, and that each of the five mediators tested alone cannot. This suggests that mediators act synergistically to activate NaN/Nav1.9 channels. The concerted action of inflammatory mediators has also been reported in the case of TRPV4 channels (Alessandri-Haber et al., 2006). The existence of crosstalk or interaction between for example PKA and PKC pathways has been documented in DRG neurons and is known to participate in inflammatory mediator-induced hyperalgesia. In addition, converging action of PKC and PKA on sodium channels has been reported (Cantrell et al., 2002). Therefore, we propose that NaN/Nav1.9 is activated by the synergistic action of the inflammatory mediators through converging signaling pathways, the nature of which remains to be established. Our data further suggest that NaN/Nav1.9 contributes specifically to inflammatory pain because its activation requires concordant stimulation of multiple signaling pathways, a condition not easily achieved by the action of a single inflammatory mediator but more likely to occur in inflamed tissues. This inference is corroborated by the observation that Nav1.9-null mice show no alteration in acute pain behaviors, but instead exhibit deficit in pain sensation after peripheral inflammation (Priest et al., 2005; Amaya et al., 2006).

To test the specific contribution of NaN/Nav1.9 channels to the firing pattern of DRG neurons, we compared the electrophysiological properties of wild-type nociceptors, in which NaN/Nav1.9 could be identified, to those of Nav1.9-null nociceptors. In these recordings, modulation of outward currents was first occluded by previous blockade of K^+ conductances (using internal Cs^+). Upregulated NaN/Nav1.9 by GTPγ-S and inflammatory soup caused increased excitability in small DRG cells. Upregulated NaN/Nav1.9 significantly lowers the threshold for excitability in small DRG neurons, as evidenced by the reduced stimulus necessary to evoke action potentials. In addition, upregulated NaN/Nav1.9 underlies plateau depolarization, often resulting in a burst of action potentials. SNS/Nav1.8-generating action potentials are ideally suited to crown NaN/Nav1.9-mediated plateau potentials due to their rapid repriming characteristics and steady-state behavior (Elliott and Elliott, 1993). The combination of NaN/Nav1.9 and SNS/Nav1.8 therefore provides an ideal environment for spontaneous firing and amplification of incoming signals.

Electrophysiological impact of upregulated NaN/Nav1.9 has also been determined under more physiological conditions, that is in the absence of K^+ and Ca^{2+} channel blockers. Although the large variety of electrophysiological behaviors resulting from the upregulation of NaN/Nav1.9 was attenuated in these experimental conditions, we were able to show that potentiation of NaN/Nav1.9 still amplifies subthreshold currents, lowers the threshold of action potentials, and enhances excitability. It is therefore concluded that NaN/Nav1.9 upregulation by the inflammatory soup changed the structure of the firing pattern in nociceptors. Although modulation of NaN/Nav1.9 was always concomitant with inhibition of a persistent K^+ current, the experiments made in $Nav1.9^{-/-}$ neurons indicated that the inflammatory soup effect on NaN/Nav1.9 current was more important than its action on K^+ currents. Further experiments and modeling techniques are however necessary to completely explain the change in firing pattern induced by the inflammatory soup.

In conclusion, the present results demonstrate that NaN/Nav1.9 is crucial in the setting of inflammation. This channel is upregulated by the synergistic action of multiple inflammatory mediators, which may be particularly important in injured neurons that are subjected to a wide spectrum of inflammatory signals. NaN/Nav1.9 endows nociceptors with a subthreshold-activating inward current that can amplify depolarizing drive. A further important question is whether NaN/Nav1.9 amplifies the response to transient sensory inputs during inflammation, which may provide a mechanism for thermal and mechanical hyperalgesia.

We thank A. Fernandez for expert technical assistance.

This work was supported by the CNRS and by grants from the ANR (05-NEUR-031), ACI BCMS-2004, ACI JC-2004, ARC-INCa-2006, and the Fondation pour la Recherche Médicale.

Olaf S. Andersen served as editor.

Submitted: 30 November 2007
Accepted: 23 January 2008

REFERENCES

Akopian, A.N., L. Sivilotti, and J.N. Wood. 1996. A tetrodotoxin-resistant voltage-gated sodium channel expressed by sensory neurons. *Nature.* 379:257–262.

Alessandri-Haber, N., O.A. Dina, E.K. Joseph, D. Reichling, and J.D. Levine. 2006. A transient receptor potential vanilloid 4-dependent mechanism of hyperalgesia is engaged by concerted action of inflammatory mediators. *J. Neurosci.* 26:3864–3874.

Amaya, F., I. Decosterd, T.A. Samad, C. Plumpton, S. Tate, R.J. Mannion, M. Costigan, and C.J. Woolf. 2000. Diversity of expression of the sensory neuron-specific TTX-resistant voltage-gated sodium ion channels SNS and SNS2. *Mol. Cell. Neurosci.* 15:331–342.

Amaya, F., H. Wang, M. Costigan, A.J. Allchorne, J.P. Hatcher, J. Egerton, T. Stean, V. Morisset, D. Grose, M.J. Gunthorpe, et al. 2006. The voltage-gated sodium channel Na(v)1.9 is an effector of peripheral inflammatory pain hypersensitivity. *J. Neurosci.* 26:12852–12860.

Baker, M.D. 2005. Protein kinase C mediates up-regulation of tetrodotoxin-resistant, persistent Na^+ current in rat and mouse sensory neurones. *J. Physiol.* 567:851–867.

Baker, M.D., S.Y. Chandra, Y. Ding, S.G. Waxman, and J.N. Wood. 2003. GTP-induced tetrodotoxin-resistant Na^+ current regulates excitability in mouse and rat small diameter sensory neurones. *J. Physiol.* 548:373–382.

Benn, S.C., M. Costigan, S. Tate, M. Fitzgerald, and C.J. Woolf. 2001. Developmental expression of the TTX-resistant voltage-gated sodium channels Nav1.8 (SNS) and Nav1.9 (SNS2) in primary sensory neurons. *J. Neurosci.* 21:6077–6085.

Black, J.A., and S.G. Waxman. 2002. Molecular identities of two tetrodotoxin-resistant sodium channels in corneal axons. *Exp. Eye Res.* 75:193–199.

Blair, N.T., and B.P. Bean. 2002. Roles of tetrodotoxin (TTX)-sensitive Na^+ current, TTX-resistant Na^+ current, and Ca^{2+} current in the action potentials of nociceptive sensory neurons. *J. Neurosci.* 22:10277–10290.

Blum, R., K.W. Kafitz, and A. Konnerth. 2002. Neurotrophin-evoked depolarization requires the sodium channel Na(V)1.9. *Nature.* 419:687–693.

Bostock, H., and P. Grafe. 1985. Activity-dependent excitability changes in normal and demyelinated rat spinal root axons. *J. Physiol.* 365:239–257.

Cantrell, A.R., V.C. Tibbs, F.H. Yu, B.J. Murphy, E.M. Sharp, Y. Qu, W.A. Catterall, and T. Scheuer. 2002. Molecular mechanism of convergent regulation of brain Na(+) channels by protein kinase C and protein kinase A anchored to AKAP-15. *Mol. Cell. Neurosci.* 21:63–80.

Coste, B., N. Osorio, F. Padilla, M. Crest, and P. Delmas. 2004. Gating and modulation of presumptive NaV1.9 channels in enteric and spinal sensory neurons. *Mol. Cell. Neurosci.* 26:123–134.

Coste, B., M. Crest, and P. Delmas. 2007. Pharmacological dissection and distribution of NaN/Nav1.9, T-type Ca^{2+} currents, and mechanically activated cation currents in different populations of DRG neurons. *J. Gen. Physiol.* 129:57–77.

Cummins, T.R., S.D. Dib-Hajj, J.A. Black, A.N. Akopian, J.N. Wood, and S.G. Waxman. 1999. A novel persistent tetrodotoxin-resistant sodium current in SNS-null and wild-type small primary sensory neurons. *J. Neurosci.* 19:RC43.

Delmas, P., and B. Coste. 2003. Na^+ channel Nav1.9: in search of a gating mechanism. *Trends Neurosci.* 26:55–57.

Delmas, P., and D.A. Brown. 2005. Pathways modulating neural KCNQ/M (Kv7) potassium channels. *Nat. Rev. Neurosci.* 6:850–862.

Dib-Hajj, S., J.A. Black, T.R. Cummins, and S.G. Waxman. 2002. NaN/Nav1.9: a sodium channel with unique properties. *Trends Neurosci.* 25:253–259.

Dib-Hajj, S.D., L. Tyrrell, J.A. Black, and S.G. Waxman. 1998. NaN, a novel voltage-gated Na channel, is expressed preferentially in peripheral sensory neurons and down-regulated after axotomy. *Proc. Natl. Acad. Sci. USA.* 95:8963–8968.

Elliott, A.A., and J.R. Elliott. 1993. Characterization of TTX-sensitive and TTX-resistant sodium currents in small cells from adult rat dorsal root ganglia. *J. Physiol.* 463:39–56.

England, S., S. Bevan, and R.J. Docherty. 1996. PGE2 modulates the tetrodotoxin-resistant sodium current in neonatal rat dorsal root ganglion neurones via the cyclic AMP-protein kinase A cascade. *J. Physiol.* 495(Pt 2):429–440.

Fang, X., L. Djouhri, J.A. Black, S.D. Dib-Hajj, S.G. Waxman, and S.N. Lawson. 2002. The presence and role of the tetrodotoxin-resistant sodium channel Na(v)1.9 (NaN) in nociceptive primary afferent neurons. *J. Neurosci.* 22:7425–7433.

Fang, X., L. Djouhri, S. McMullan, C. Berry, S.G. Waxman, K. Okuse, and S.N. Lawson. 2006. Intense isolectin-B4 binding in rat dorsal root ganglion neurons distinguishes C-fiber nociceptors with broad action potentials and high Nav1.9 expression. *J. Neurosci.* 26:7281–7292.

Fjell, J., T.R. Cummins, S.D. Dib-Hajj, K. Fried, J.A. Black, and S.G. Waxman. 1999. Differential role of GDNF and NGF in the maintenance of two TTX-resistant sodium channels in adult DRG neurons. *Brain Res. Mol. Brain Res.* 67:267–282.

Gold, M.S., D.B. Reichling, M.J. Shuster, and J.D. Levine. 1996. Hyperalgesic agents increase a tetrodotoxin-resistant Na^+ current in nociceptors. *Proc. Natl. Acad. Sci. USA.* 93:1108–1112.

Gold, M.S., J.D. Levine, and A.M. Correa. 1998. Modulation of TTX-R INa by PKC and PKA and their role in PGE2-induced sensitization of rat sensory neurons in vitro. *J. Neurosci.* 18:10345–10355.

Herzog, R.I., T.R. Cummins, and S.G. Waxman. 2001. Persistent TTX-resistant Na^+ current affects resting potential and response to depolarization in simulated spinal sensory neurons. *J. Neurophysiol.* 86:1351–1364.

Hines, M.L., and N.T. Carnevale. 2001. NEURON: a tool for neuroscientists. *Neuroscientist.* 7:123–135.

Hodgkin, A.L., and A.F. Huxley. 1952. A quantitative description of membrane current and its application to conduction and excitation in nerve. *J. Physiol.* 117:500–544.

Khasar, S.G., M.S. Gold, and J.D. Levine. 1998. A tetrodotoxin-resistant sodium current mediates inflammatory pain in the rat. *Neurosci. Lett.* 256:17–20.

Kwong, K., and L.Y. Lee. 2005. Prostaglandin E2 potentiates a TTX-resistant sodium current in rat capsaicin-sensitive vagal pulmonary sensory neurones. *J. Physiol.* 564:437–450.

Maruyama, H., M. Yamamoto, T. Matsutomi, T. Zheng, Y. Nakata, J.N. Wood, and N. Ogata. 2004. Electrophysiological characterization of the tetrodotoxin-resistant Na^+ channel, Na(v)1.9, in mouse dorsal root ganglion neurons. *Pflugers Arch.* 449:76–87.

Matsutomi, T., C. Nakamoto, T. Zheng, J. Kakimura, and N. Ogata. 2006. Multiple types of Na^+ currents mediate action potential electrogenesis in small neurons of mouse dorsal root ganglia. *Pflugers Arch.* 453:83–96.

Padilla, F., M.L. Couble, B. Coste, F. Maingret, N. Clerc, M. Crest, A.M. Ritter, H. Magloire, and P. Delmas. 2007. Expression and localization of the Nav1.9 sodium channel in enteric neurons and in trigeminal sensory endings: implication for intestinal reflex function and orofacial pain. *Mol. Cell. Neurosci.* 35:138–152.

Passmore, G.M., A.A. Selyanko, M. Mistry, M. Al-Qatari, S.J. Marsh, E.A. Matthews, A.H. Dickenson, T.A. Brown, S.A. Burbidge, and D.A. Brown. 2003. KCNQ/M currents in sensory neurons: significance for pain therapy. *J. Neurosci.* 23:7227–7236.

Priest, B.T., B.A. Murphy, J.A. Lindia, C. Diaz, C. Abbadie, A.M. Ritter, P. Liberator, L.M. Iyer, S.F. Kash, M.G. Kohler, et al. 2005. Contribution of the tetrodotoxin-resistant voltage-gated sodium

channel NaV1.9 to sensory transmission and nociceptive behavior. *Proc. Natl. Acad. Sci. USA*. 102:9382–9387.

Renganathan, M., T.R. Cummins, and S.G. Waxman. 2001. Contribution of Na(v)1.8 sodium channels to action potential electrogenesis in DRG neurons. *J. Neurophysiol.* 86:629–640.

Rugiero, F., M. Mistry, D. Sage, J.A. Black, S.G. Waxman, M. Crest, N. Clerc, P. Delmas, and M. Gola. 2003. Selective expression of a persistent tetrodotoxin-resistant Na^+ current and NaV1.9 subunit in myenteric sensory neurons. *J. Neurosci.* 23:2715–2725.

Rush, A.M., and S.G. Waxman. 2004. PGE2 increases the tetrodotoxin-resistant Nav1.9 sodium current in mouse DRG neurons via G-proteins. *Brain Res.* 1023:264–271.

Stys, P.K., H. Sontheimer, B.R. Ransom, and S.G. Waxman. 1993. Noninactivating, tetrodotoxin-sensitive Na^+ conductance in rat optic nerve axons. *Proc. Natl. Acad. Sci. USA*. 90:6976–6980.

Zheng, T., J. Kakimura, T. Matsutomi, C. Nakamoto, and N. Ogata. 2007. Prostaglandin E2 has no effect on two components of tetrodotoxin-resistant Na^+ current in mouse dorsal root ganglion. *J. Pharmacol. Sci.* 103:93–102.